CHAPTER 13

Styrene–Acrylonitrile Copolymer Montmorillonite Nanocomposite: Processing, Characterization and Flammability

JEFFREY W. GILMAN,[1] SERGE BOURBIGOT,[2] SÉVERINE BELLAYER,[1] HOLLY STRETZ[3] AND DONALD R. PAUL[3]

[1]Fire Science Division, BFRL, National Institute of Standards and Technology, Gaithersburg, MD-20899, U.S.A.
[2]PERF, UPRES EA 1040, École Nationale Supérieure de Chimie de Lille (ENSCL), F-59650 Villeneuve d'Ascq, France (Guest Researcher at Fire Science Division, BFRL, NIST, Gaithersburg, MD-20899, U.S.A.
[3]The University of Texas, Austin, TX-78712, U.S.A.

13.1 Introduction

Interest in polymer clay nanocomposites has increased significantly in recent years. Property improvements include better mechanical properties, better barrier properties, lower water absorption and reduced flammability.[1–6] To achieve these properties, mica-type layered silicates, such as montmorillonite (MMT), are generally dispersed at the nanoscale in the polymer to yield the so-called "nanocomposite".

The pioneering work of Gilman *et al.* demonstrated that the presence of montmorillonite clay produces a substantial improvement in fire performance in polymeric matrices such as polystyrene and polyamides.[5–7] The purpose of this work is to investigate the melt-processing of styrene-acrylonitrile copolymer (SAN) with MMT clays and the influence of the clay on mechanical properties and on fire performance of SAN. Our work is included in a larger project aimed at understanding the flame retardancy of ABS. Computer housings are typically made from acrylonitrile-butadiene-styrene (ABS) polymer and related blends,

and these polymers must meet safety standards. The SAN polymer discussed here is a model system for the study of ABS/clay systems, since the multi-phase ABS consists of an SAN matrix embedded with rubber particles. Our concern here is to simplify the system to study the nanodispersion of the clay in SAN. In addition, we will discuss in future publications how the clay dispersion and organoclay compatibilizer affect flammability in SAN and ABS.

The first part of this chapter is devoted to the characterization by X-ray diffraction (XRD), transmission electronic microscopy (TEM) and solid-state nuclear magnetic resonance (NMR) of the nanocomposites. These characterization methods are complementary, but it should be pointed out that solid state NMR characterization has not been previously reported for SAN/MMT, and that the advantage of NMR characterization of nanocomposites is that the sample size probed is much larger (and therefore more representative of a bulk dispersion) than either XRD or TEM. Together, these methods will provide an overview of the dispersion of the clay in SAN. Then, tensile properties and flammability performance evaluated by mass loss calorimetry will be examined and discussed.

13.2 Experimental[a]

13.2.1 Preparation of Nanocomposites

MMT originated from Southern Clay Products, Inc (Gonzales, TX, USA). The starting material, sodium-MMT, was commercially modified using methyl, tallow, bis-2-hydroxyethyl, quaternary ammonium chloride (Cloisite 30B). SAN copolymer, containing 25 mass% acrylonitrile (SAN-25) and formulated for computer housing, was supplied by Dow Chemical.

Polymer melt-direct intercalation is an approach to making polymer layered silicate nanocomposites by using conventional polymer extrusion. The optimized processing temperature for best dispersion was determined to be 220°C.[8] SAN-25 was melt-mixed with the clay using a co-rotating twin-screw extruder (Haake, screw L/D = 10, diameter = 35 mm) at 280 rpm. These conditions on this extruder produce fully exfoliated nylon-6/montmorillonite nanocomposites.[9] The clay loadings (Cloisite 30B) were 2.2, 4.2, 6.2 and 7.9 wt% true silicates. The true silicate concentration is determined by heating the dry, post-extrusion pellets in a muffle furnace to 900°C for 45 min, and correcting for structural rearrangement by dividing the ash percentage by 0.935 (the silicate

[a] This work was carried out by the National Institute of Standards and Technology (NIST), an agency of the U.S. government and by statute is not subject to copyright in the United States. Certain commercial equipment, instruments, materials or companies are identified in this paper in order to adequately specify the experimental procedure. This in no way implies endorsement or recommendation by NIST. The policy of NIST is to use metric units of measurement in all its publications, and to provide statements of uncertainty for all original measurements. In this document, however, data from organizations outside NIST are shown, which may include measurements in non-metric units or measurements without uncertainty statements.

rearrangement results in 6.5% loss of structural water). Organoclay content can then be calculated from the true silicate content as reported here by using:

$$\text{organoclay (\%)} = \frac{0.935 \times \text{MMT}}{\left[1 - \text{LoI}/100\right]}$$

where LoI is the loss on ignition for the dry organoclay (30% for Cloisite 30B), and MMT is the true silicate mass percentage.

13.2.2 NMR Spectroscopy

Measurements were conducted using a Bruker Avance 300 spectrometer (Bruker BioSpin Corp., Billerica, MA) operating at 7.05 T. Proton spectra at 300 MHz were obtained using a 5 mm low proton-background CRAMPS[10] (combined rotation and magic-angle spinning) probe (Doty Scientific of Columbia, SC).

Even though we recognized the strong effect of oxygen (it will be commented in the following),[11] proton longitudinal relaxation times (T_1^H) of oxygen-containing samples were obtained using the inversion–recovery sequence with direct proton observation[12] in a ZrO_2 rotor. For purposes of time efficiency, only the delay time, τ_{null}, was determined. The latter is the delay time where, after inversion, magnetization passes through zero on its way back to the Boltzmann equilibrium level. From τ_{null}, a lower limit for T_1^H was calculated *via* the relationship $T_1^H = \tau_{null}/\ln 2$. This relationship assumes full initial inversion of the magnetization and single-exponential recovery. The paramagnetic contribution to T_1^H originating from the MMT clay (paramagnetic Fe^{3+} is embedded in the aluminosilicate layers of the MMT) normally produces a slightly accelerated early decay relative to the typically exponential behavior seen at longer times; hence, this relationship systematically yields a lower limit to the T_1^H than would describe this longer time behavior. In any case, all samples had equilibrated with O_2 and had aged for at least one month. Standard uncertainties for τ_{null} measurements are ±2.5% of the given value.

13.2.3 Transmission Electron Microscopy

All samples were ultra-microtomed with a diamond knife on a Leica Ultracut UCT microtome to give sections with a nominal thickness of 70 nm. The sections were transferred from water (room temperature) to Cu grids of 400 mesh. Bright-field TEM images of nanocomposites were obtained at 120 kV under low-dose conditions with a Philips 400T electron microscope, using Kodak SO-163 film. Low-magnification images were taken 22,000×. High-magnification images were taken at 100,000×. The materials were sampled by taking several images of various magnifications over 2–3 sections per grid to ensure that analysis was based on a representative region of the sample.

13.2.4 Tensile Properties

Injection molding of tensile test bars (ASTM D638) was performed on an Arburg Allrounder 305-210-700 injection molding machine. Test specimens were molded at a barrel temperature of 260°C, and a mold temperature of 80°C. Mechanical testing was performed on an Instron model 1137 at a strain rate of 0.51 cm min^{-1}, and moduli data were evaluated using an extensometer with a 2.5 cm gauge length. Standard deviations for 5 or more test bars were under 10% of the mean for moduli. Standard deviations on the tensile strength at break and strain at break increased with clay percentage up to a maximum of 15% of the mean.

13.2.5 Cone Calorimetry by Mass Loss Calorimeter

FTT (Fire Testing Technology) mass loss calorimeter was used to carry out measurements on samples following the procedure defined in ASTM E 906. The equipment is identical to that used in oxygen consumption cone calorimetry (ASTM E-1354-90), except that a thermopile in the chimney is used to obtain heat release rate (HRR) rather than employing the oxygen consumption principle. Mass loss readings are performed simultaneously by ASTM E-1354, and serve as a benchmark of the heat release rate values obtained in this manner. ASTM E 906 is a screening method, and results in an internally representative set of data. For comparison, fully scaleable peak heat release rates from ASTM E-1354 for non-FR ABS grades range from 800[13] to 1000 kW m^{-2} [14] at an external heat flux of 35 kW m^{-2}. The procedure involved exposing specimens measuring 100 × 100 × 3 mm in horizontal orientation. An external heat flux of 35 kW m^{-2} was used for running the experiments. This flux corresponds to common heat flux in mild fire scenario.[15,16] The MLC calorimeter was used to determine heat release rate (HRR). When measured at 35 kW m^{-2}, HRR is reproducible to within ±10%. The cone data reported here the average of three replicated experiments.

13.3 Results and Discussion

13.3.1 Characterization by XRD and TEM

TEM images of SAN-25 MMT nanocomposites containing 2.2, 4.2, 6.2 and 7.9 wt% of true silicate are shown at low magnification (Figures 1a to 4a) and at higher magnification (Figure 1b to 4b).

At low magnification, the images reveal that clay is well and evenly dispersed in all nanocomposites. At higher magnification, all samples exhibit dispersion of multi-layer stacks (tactoids) of individual MMT layers that range from 2 to 10 layers in size. Some individual MMT layers can be also distinguished.

The samples are not all similar; the nanostructure of nanocomposite (size of the tactoids) appears qualitatively to depend on the loading in organo-clay although a quantitative analysis of the distribution has not yet been attempted. We can observe that, as the clay loading is increased, larger tactoids seem to become more prevalent. This trend has been suggested in the literature,[17] *i.e.*

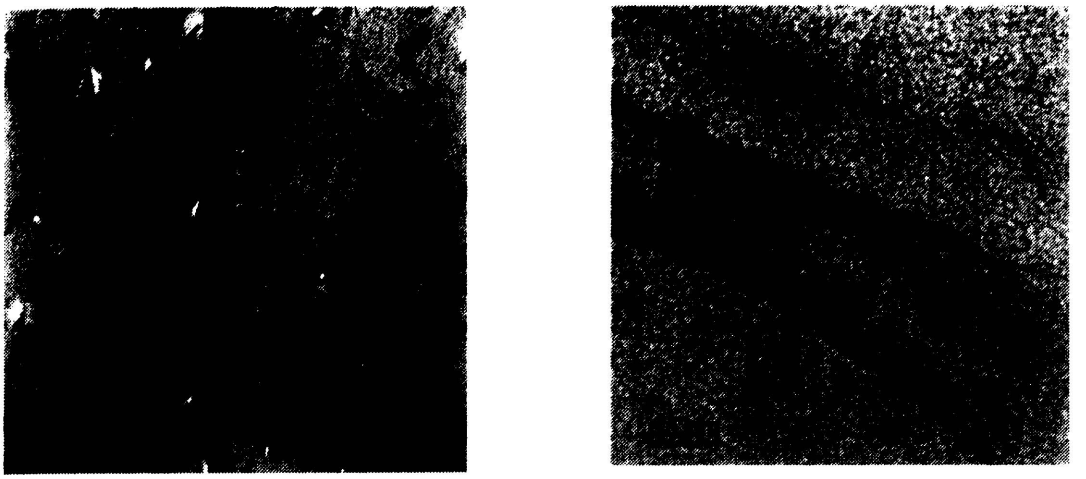

Figure 1 *TEM images at low* (a) *and high* (b) *magnification of SAN-25 MMT nanocomposites at 2.2 wt% silicate*

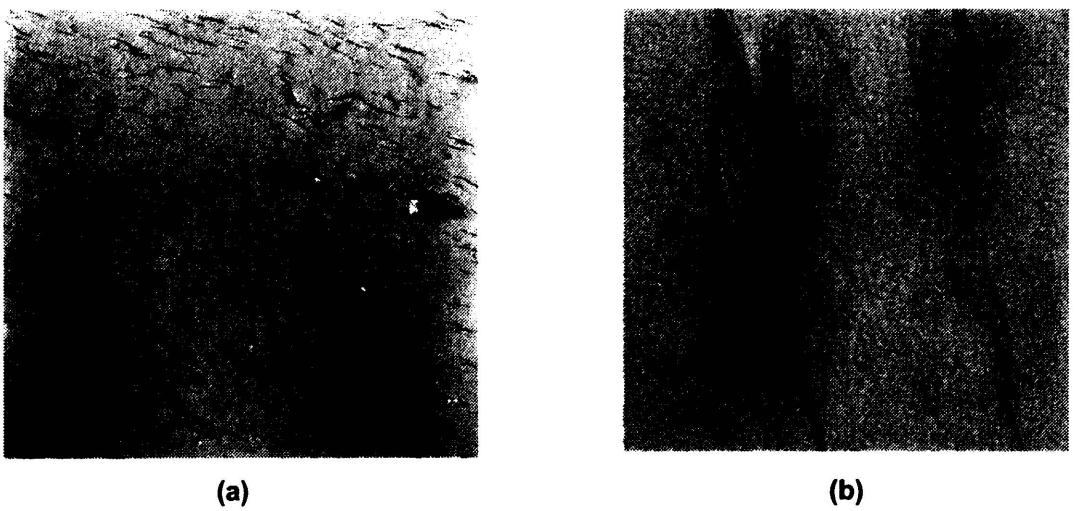

Figure 2 *TEM images at low* (a) *and high* (b) *magnification of SAN-25 MMT nanocomposites at 4.2 wt% silicate*

relatively high loading in clay favors the agglomeration of MMT platelets. In addition to this, XRD spectra (not shown)[8] reveal diffraction peaks in the low-angle region giving a *d*-spacing falling between 3.1 and 3.25 nm. The *d*-spacing of the pure organo-clay is 1.75 nm and this result suggests that at least a part of the nanocomposite has an intercalated structure. From TEM and XRD, we may conclude that the nanocomposites have a mixed intercalated/exfoliated structure regardless of the loading.

13.3.2 T_1^H of Nanocomposite

An approach has been developed at NIST by VanderHart *et al.* using solid-state NMR to characterize the nanodispersion of clay in polymers.[18–20] The method is

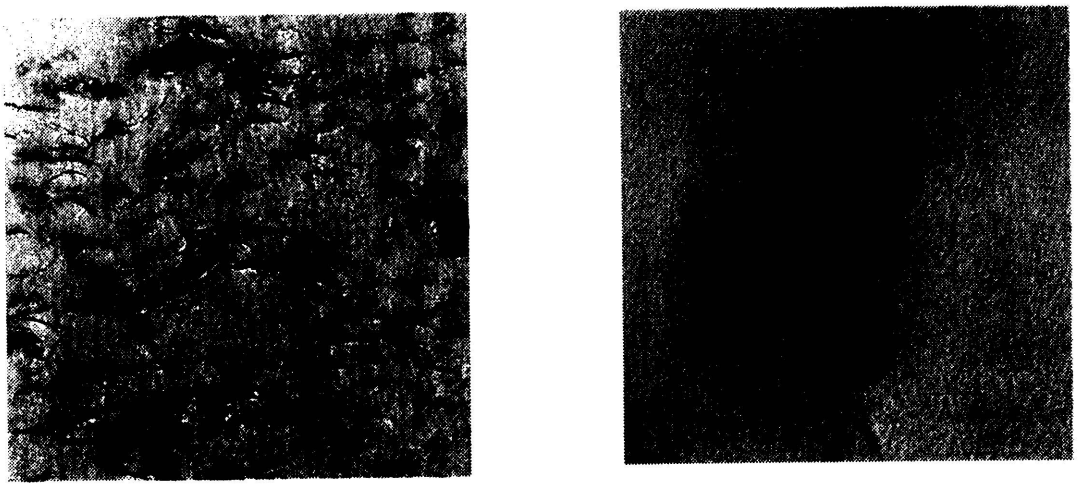

(a) (b)

Figure 3 *TEM images at low (a) and high* (b) *magnification of SAN-25 MMT nanocomposites at 6.2 wt% silicate*

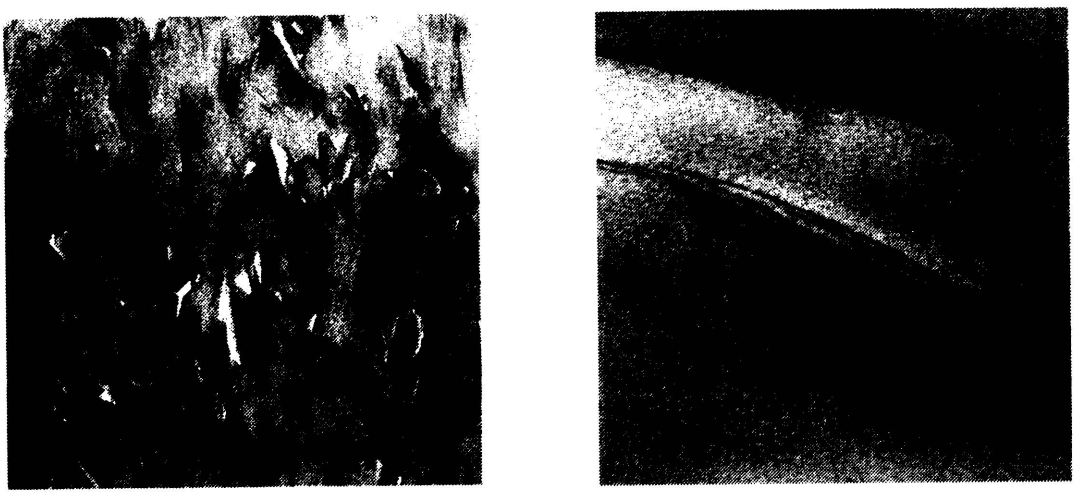

(a) (b)

Figure 4 *TEM images at low (a) and high* (b) *magnification of SAN-25 MMT nanocomposites at 7.9 wt% silicate*

based on T_1^H measurement. It utilizes two effects: (1) the paramagnetic character of this MMT, which directly reduces the T_1^H of nearby protons, and (2) spin diffusion, whereby this locally enhanced relaxation propagates to more distant protons. As reported,[11,21,22] the adsorption of paramagnetic oxygen on aromatic polymers causes a major shortening of T_1^H. This was shown previously for polystyrene but we suspect the same effect for SAN polymer because of the presence of phenyl ring in the repeat unit of this polymer. The amount of adsorbed oxygen is a function of the chemical nature of the polymer, its molecular packing, molecular motion and temperature. Thus, in addition to the sensitivity of T_1^H to clay dispersion, any other changes that might affect oxygen solubility or dynamics could also influence T_1^H. The purpose here is to use the shortening of T_1^H measured in SAN-25/MMT nanocomposites to get an estimation of the

Table 1 *NMR, XRD and TEM characterization of oxygenated SAN-25/MMT nanocomposites*

Polymer/MMT nanocomposite	*OrganoMMT concentration* (wt%)	*True silicate concentration* (wt%)	T_1^H (τ_{null}/ln2) (s)	*XRD/TEM conclusions*
SAN-25	0	0	1.77	–
SAN-25/3	3.0	2.2	1.14	Well and evenly dispersed, exfoliated/intercalated with small tactoids (2–3 layers)
SAN-25/6	5.6	4.2	0.84	Well and evenly dispersed, exfoliated/intercalated with small tactoids (3–5 layers)
SAN-25/8	8.3	6.2	0.63	Well and evenly dispersed, exfoliated/intercalated with small tactoids (3–8 layers)
SAN-25/11	10.6	7.9	0.54	Well and evenly dispersed, exfoliated/intercalated with small tactoids (3–10 layers)

nanodispersion of the clay in the polymer. In a future paper,[23] we will discuss the effect of oxygen and propose a quantitative approach for determining the nanodispersion using solid-state NMR.

Table 1 shows T_1^H data, obtained from τ_{null}, for our oxygen containing SAN-25/MMT nanocomposites. T_1^Hs of samples are shortened by the paramagnetic character of the clay.

All T_1^H data of SAN-25/MMT nanocomposites fall between 1.14 and 0.54 s (T_1^H of the pure SAN-25 is 1.77 s). T_1^H decreases with increasing MMT concentration for all nanocomposites, and depends on both the MMT concentration and the quality of the dispersion. It decreases noticeably for each sample compared to the pure SAN-25 and, as expected, the higher the MMT concentration, the shorter T_1^H is. By analogy with our previous work with nylon-6/clay nanocomposites[20] and PS/MMT nanocomposites,[11] the T_1^Hs of our samples suggest a modestly good dispersion of the clay. Here, a good correlation is found between T_1^Hs, and XRD and TEM conclusions. However, such a result should be considered only if secondary issues such as the presence of residual monomer do not modify the solubility of oxygen. Indeed, effects like residual monomer, large amounts of organo-modifier, or even small amounts, could potentially lead to an inappropriate conclusion about the dispersion of the clay if one does not properly take account of such phenomena. Nevertheless, we checked the Bloch spectra (not shown), and no degradation of SAN-25 or of the organo-modifier of the clay could be detected, *i.e.* there was no NMR evidence of additional mobile species present in our samples.

13.3.3 Tensile Properties

Figure 5 shows the tensile properties of SAN-25/MMT nanocomposites. Young's modulus clearly increases as a function of the MMT concentration but,

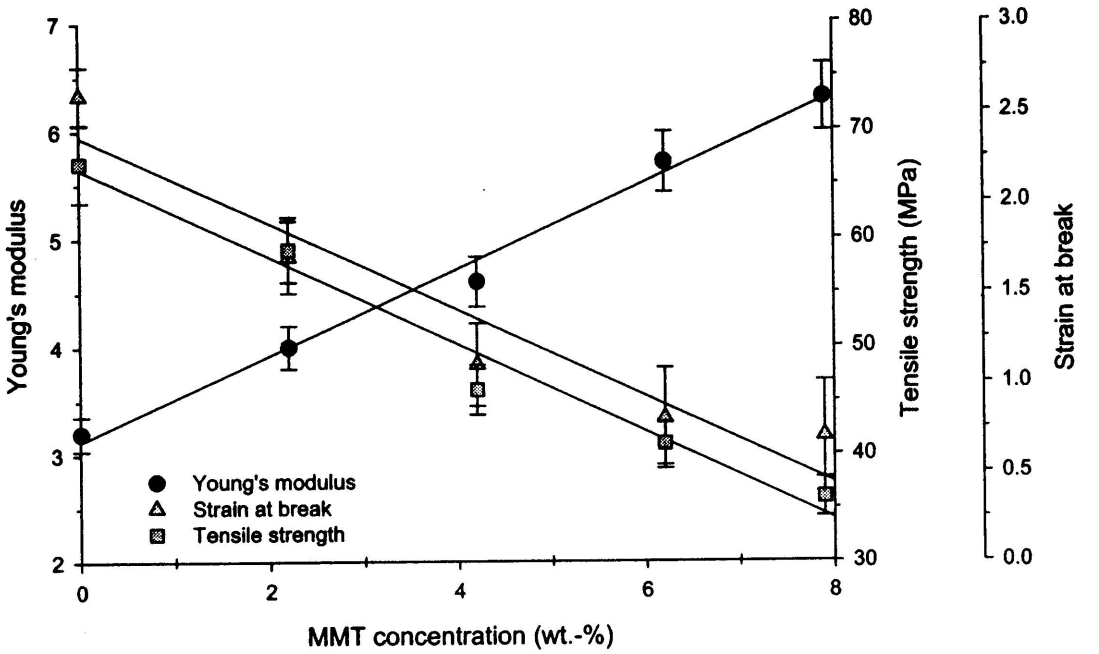

Figure 5 *Young's modulus, tensile strength and strain at break vs. MMT concentration of SAN-25/MMT nanocomposites*

concurrently, tensile strength and strain at break decrease. Young's modulus of SAN-25/MMT nanocomposites is substantially superior to that of neat SAN-25 due to the reinforcement by the clay platelets. The modulus exhibits a linear behavior *versus* the MMT content in the polymer. Surprisingly, tensile strength drops with higher clay loading. Most literature reports show an increase in strength at yield with clay loading,[14] but the SAN/MMT samples broke in a brittle manner before yield, and comparison to a ductile matrix is then not valid in terms of the strain regime. Both tensile strength and strain at break show a linear decrease at low clay loadings, suggesting the presence of small agglomerates in the polymer, as reported elsewhere.[17] This dependence appears to plateau at higher loadings, but the standard deviation also increases with loading, making the trend difficult to evaluate. The nature of the variation of tensile strength with loading for nanocomposites with a brittle matrix (*i.e.* SAN) is not completely understood. All nanocomposites exhibit an intercalated structure with some exfoliation and tactoids of small size. We also observed a linear dependence of the tensile modulus properties *versus* clay content for the range of loading tested. We have, therefore, a "filler effect" increasing the stiffness but decreasing the tensile strength of the nanocomposites.

13.3.4 Flammability Properties

Peak of heat release rate (PHRR) of polystyrene is reduced upon addition of clay;[24,25] however, to our knowledge, no published data are available for melt-processed SAN nanocomposites. Figure 6 shows significant reductions in PHRR in SAN-25 as a function of clay content. This reduction is strongly enhanced at higher clay loading. As an example, PHRR is decreased by 36%

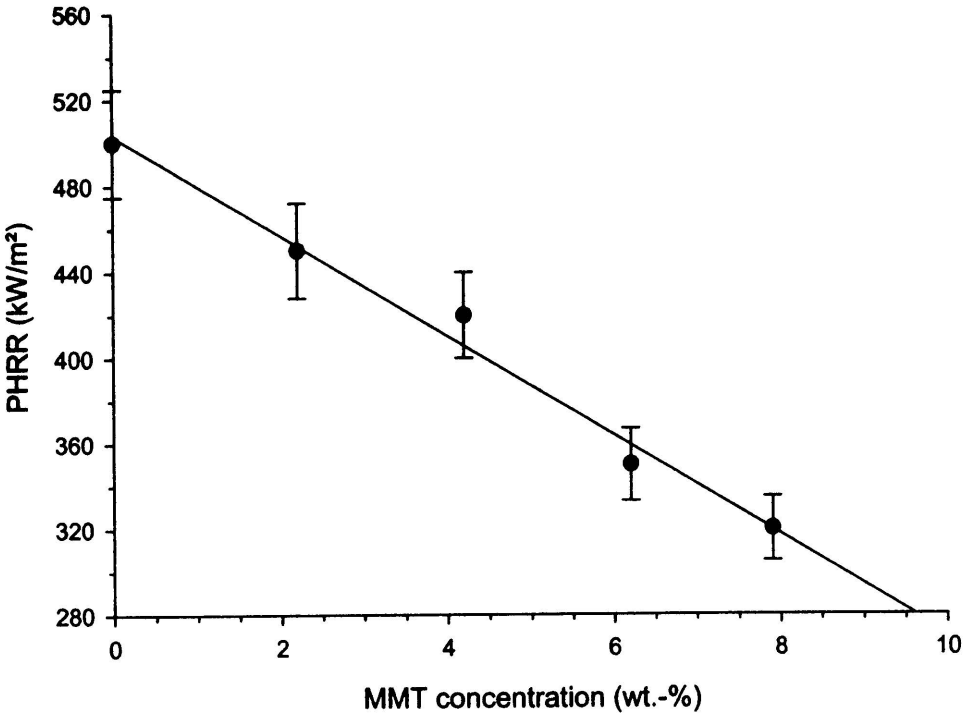

Figure 6 *Peak of heat release rate (PHRR) vs. MMT concentration of SAN-25/MMT nanocomposites*

at 4.6 wt% in MMT concentration. The suggested mechanism by which clay nanocomposites function involves the formation of a surface layer that serves as a potential barrier to both mass and energy transport.[24] The higher the initial concentration of clay, the thicker (and more insulating) is the ceramic-like layer that forms at the decomposing surface of the burning sample, with due consideration for homogeneity and integrity of the forming layer.

13.4 Conclusion

This work has characterized the dispersion of montmorillonite clay in SAN-25 and evaluated the mechanical properties and the reaction to fire of SAN-25/MMT nanocomposites. The nanodispersion has been characterized by XRD, TEM, and solid-state NMR. SAN-25/MMT nanocomposites reveal an intermediate morphology, *i.e.* an intercalated structure with some exfoliation and with the presence of small tactoids whatever the loading in MMT is. The presence of clay in SAN-25 leads to a "filler effect" that increases the stiffness but decreases the tensile strength of the nanocomposites. It also leads to a significant decrease of peak of heat release rate (up to 36%) as measured by mass loss calorimetry.

13.5 References

1. M. Alexandre and P. Dubois, *Mat. Sci. Eng., R.* 2000, **28(1–2)**, 1–63.
2. Y. Kojima, A. Usuki, M. Kawasumi, A. Okada, Y. Fukushima, T. Kurauchi and O. Kamigaito, *J. Mater. Res.*, 1993, **8(5)**, 1185–1189.

3. A. Okada, Y. Fukushima, M. Kawasumi, S. Inagaki, A. Usuki, S. Sugiyama, T. Kurauchi and O. Kamigaito, *US Patent 4,739,007*, 1988.
4. P.B. Messersmith and E.P. Giannelis,. *J. Polym. Sci. A., Polym. Chem.*, 1995, **33(7)**, 1047–1057.
5. J.W. Gilman, T. Kashiwagi and J.D. Lichtenhan, *SAMPE J.*, 1997, **33**, 40–46.
6. J.W. Gilman, *Appl. Clay Sci.*, 1999, **15(1–2)**, 31–49.
7. J.W. Gilman, T. Kashiwagi, E.P. Giannelis, E. Manias, S. Lomakin, J.D. Lichtenhan and P. Jones, in *Fire Retardancy of Polymers – The Use of Intumescence*, M. Le Bras, G. Camino, S. Bourbigot, and R. Delobel (eds.), The Royal Society of Chemistry, Cambridge, 1998, pp. 223–235.
8. H. Stretz, *Preliminary Proposal 2002*, University of Texas, Austin.
9. T.Fornes, P.J. Yoon, H. Keskkula and D.R. Paul, *Polymer*, 2001, **42**, 9929–9940.
10. L.M. Ryan, R.E. Taylor, A.J. Paff and B.C. Gerstein, *J. Chem. Phys.*, 1980, **72**, 508–515.
11. S. Bourbigot, D.L. VanderHart, J.W. Gilman, W.H. Awad, R.D. Davis, A.B. Morgan and C.A. Wilkie, *J. Polym. Sci. B, Polym. Phys.*, in press.
12. T.C. Farrar and E.D. Becker, in *Pulse and Fourier Transform NMR*, Academic Press, New York, 1971, pp. 20f.
13. A. Grand, in *Heat Release Calorimetry Evaluation of Fire Retardant Polymer Systems*, 42nd Intl. SAMPE Proceedings, 1997, Volume 5.
14. M.J. Scudmore, P.J. Briggs and F.H. Prager, *Fire Mater.*, 1991, **15**, 65–84.
15. V. Babrauskas, *Development of Cone Calorimeter – A bench scale rate of heat release based on oxygen consumption*, NBS-IR 82-2611, US Nat. Bur. Stand., Gaithersburg, 1982.
16. V. Babrauskas, *Fire Mater.*, 1984, **8(2)**, 81.
17. J.-H. Chang, Y.U. An and G.S. Sur, *J Polym. Sci, Part B: Polym. Phys.*, 2003, **41**, 94.
18. D.L. VanderHart, A. Asano and J.W. Gilman, *Macromolecules,* 2001, **34**, 3819–3822.
19. D.L. VanderHart, A. Asano and J.W. Gilman, *Chem. Mater.*, 2001, **13**, 3781–3795.
20. D.L. VanderHart, A. Asano and J.W. Gilman, *Chem. Mater.*, 2001, **13**, 3796–3809.
21. D.Capitani, C. de Rosa, A. Ferrando, A. Grassi and A.L. Segre, *Macromolecules*, 1992, **25**, 3874–3880.
22. D. Capitani, A.L. Segre and J.S. Blicharski, *Macromolecules*, 1995, **28**, 1121–1128.
23. S. Bourbigot, D.L. VanderHart, J.W. Gilman, S. Bellayer, H. Stretz and D.R. Paul, manuscript in preparation.
24. J. Zhu, A.B. Morgan, F.J. Lamelas and C.A. Wilkie, *Chem. Mater.*, 2001, **13**, 3774–3780.
25. J. Zhu, F.M. Uhl, A.B. Morgan and C.A., Wilkie, *Chem. Mater.*, 2001, **13**, 4649–4654.